Nanoscale

ROYAL SOCIETY OF CHEMISTRY

PAPER

View Article Online
View Journal | View Issue

Check for updates

Cite this: *Nanoscale*, 2020, **12**, 6736

A mechanically bendable and conformally attachable polymer membrane microlaser array enabled by digital interference lithography

Wenbin Huang, [a,b] Xin-Jun Zhang,[a] Tianchi Yang,[a] Shaolong Wu, [a] Xiaofei Yang,*[a] Yan-Hua Liu *[a] and Linsen Chen[a]

Received 31st December 2019,
Accepted 4th March 2020

DOI: 10.1039/c9nr10970f

rsc.li/nanoscale

The progressive miniaturization and thinning of photonic devices would enable the realization of multifunctional photonic integrated circuits and expand the application frontier to novel fields including wearable and disposable electronics. Herein, we have demonstrated a mechanically bendable and conformally attachable polymer membrane microcavity laser array using digital interference lithography. The developed lithography system could distribute a number of subwavelength grating pixels with both high efficiency (1k pixels per second) and excellent versatility (ease of control in the pixel size, spacing, and grating periodicity) as the microcavity laser array, in which a pair of subwavelength gratings constitutes a distributed Bragg resonator microcavity *via* coherent interference, furnishes a vertically emitting microcavity laser array for convenient light coupling and utilization. The microlaser array polymer membrane presented a total thickness of only 30 μm with excellent performance stability and reliability against long time operation and harsh environmental conditions, which could be further reversibly stretched, repeatedly bendable and conformally attached onto rounded or irregular surfaces or biological tissues with no degradation in single-mode or low-threshold characteristics, paving a way for on-chip optical functionalization toward wearable electronics and outdoor environmental monitoring applications.

Introduction

Photonic devices are evolving towards miniaturization with the final goal of integrating a number of functional components onto a compact chip, producing photonic integrated circuits (PICs) with low requirements for energy consumption and high degrees of functionality, paving ways for on-chip applications such as optical communication, high-sensitivity sensing, logic nanophotonics, optical data processing, high-resolution imaging, *etc*.[1–3] Recently, driven by the growing demand of fabricating PICs with high portability, bendability, lightweight, and low manufacturing cost, there has been growing interest in developing flexible and miniaturized photonic devices that can be mechanically deformed without compromising the performance, aiming to expand the application frontier of PICs toward new areas such as wearable or disposable electronics.[4–7] To achieve this ultimate goal, there has been extensive research activities in exploring and developing nanoscale lasers with both high optoelectrical performance and high mechanical roubustness.[8–10] In this regard, organic semiconductors appear to be quite suitable, because of their large simulated emission cross-sections, excellent flexibility, solution processability and inherent compatibility with plastic substrates, in combination with various microcavity resonator designs including the distributed feedback (DFB), the whispering gallery and the distributed Bragg reflector (DBR), to furnish mechanically flexible,[11,12] low threshold,[13,14] wavelength tunable[15,16] and even white-emitting[17] microlasers. Substantive endeavours have been devoted to reducing the thickness of polymer microlasers by throwing away the flexible substrates, which is achieved by detaching the cavity-structured gain material film from the supporting substrate after dissolving the sacrificial layer in a suitable solvent, thus exhibiting excellent flexibility and transplantation.[18,19] However, the ultra-thin polymer laser device is extremely mechanically fragile and difficult to handle which is often suspended over a hole in a supporting substrate, and furthermore, the device performance is unstable with operation time and susceptible to environmental conditions, as the organic gain medium is directly exposed to oxygen and moisture.[20]

Apart from improving the mechanical flexibility and bendability, the miniaturization of these polymer lasers provides

[a]*School of Optoelectronic Science and Engineering & Collaborative Innovation Center of Suzhou Nano Science and Technology, Soochow University, Suzhou 215006, China. E-mail: yangxiaofei@suda.edu.cn, yhliu@suda.edu.cn*
[b]*State Key Lab of Applied Optics, Changchun Institute of Optics, Fine Mechanics and Physics, Chinese Academy of Sciences, Changchun, Jilin 130033, China*

the possibility to obtain the laser array on the nano- and micro-scale for its convenient integration in PIC devices,[21,22] which could be distributed across the photonic chip on demand with well-designed laser parameters, such as the lasing wavelength, the device size and the emitting direction, motivating research efforts to explore techniques with the potential of parallel matrix fabrication. As a direct approach, one could extend the single laser fabrication route simply by placing a number of microcavity polymer lasers (laser pixels) on the same substrate, for example, the electron beam lithography (EBL) technique has been utilized to provide pixelated subwavelength gratings for obtaining the DFB polymer laser array, where the fabrication efficiency and stability is greatly limited by its serial fabrication nature.[23–27] One could also obtain polymer micro-pillars, sandwiched between two dielectric mirrors by the laser direct writing technique, acting as the polymer laser array emitting multi-wavelength lasing, by confining the light in each micro-pillar *via* the Fabry–Perot mechanism.[28] In addition, an organic crystal array with micrometer-scale squares can be fabricated by cutting the single-crystalline organic microbelt into pieces by the two-photon processing technique,[29] producing light resonation in the squares by the edge reflections, resulting in single wavelength lasing emitting from the two edges. Moreover, low-threshold microring laser arrays with unit components of precise positioning and tunable size have been fabricated in a highly efficient and versatile manner by manipulating the dewetting process in the triphase contact line using a micropillar template[30] or the ink-jet printing technique in combination with the coffee-ring effect,[31] albeit each microlaser with a multiple mode characteristic. As a result, there is still an urgent demand for developing fabrication techniques to obtain polymer microcavity laser arrays featuring high fabrication efficiency, precise positioning, single-mode laser operation and low working threshold, as it may provide a new platform for the monolithic integration of microlaser arrays with PICs to explore novel on-chip applications in areas of displays, sensing and spectroscopy.

In this work, we have proposed and demonstrated a mechanically flexible and conformally attachable microcavity laser array membrane using the digital interference lithography technique. The proposed lithography system could distribute pixelated subwavelength gratings with both high efficiency (1k pixels per second) and flexibility in controlling the position, the spacing, the size and the period of each pixelated grating, where a pair of subwavelength gratings yields a pixelated microcavity laser by introducing the DBR mechanism, presenting as a novel and powerful platform to provide microcavity polymer laser arrays for planar functionalization and integration. In addition, we have also provided a novel nanoimprinting approach to achieve the microcavity laser array membrane with high robustability and mechanical flexibility, which is realized through peeling the thin nanostructured UV-curable film from the hard nickel (Ni) mold after UV curing, followed by coating the active film and the encapsulation layer, thus furnishing a free-standing microcavity polymer membrane (20–40 μm) with both bendability and transplantability. The microlaser array exhibits excellent laser performance, including stable single-mode lasing and low operating threshold (around 15 μJ cm^{-2}) after reversible stretching, repeated bending and attaching circles, acting as a robust and low-cost microcavity laser membrane for integration in flexible PICs to explore its practical potential in numerous applications.

Subwavelength gratings are very important components for photonic applications in beam steering, light confinement, optical coupling, *etc*. Such gratings could also be exploited as microcavity resonators by introducing the DFB mechanism *via* coherent backward scattering or the DBR mechanism by coherent interference at the selective reflection wavelength, which inherently have advantages of ease of integration, low working threshold, high beam directionality, and excellent wavelength purity, acting as an effective approach to realize the microcavity laser array. The development of such a laser array was severely limited by the current manufacturing techniques, as it often requires the EBL to complete the task. In this work, we have developed a system with both high fabrication efficiency and flexibility in distributing the pixelated subwavelength gratings based on the so-called digital interference lithography. In this system (Fig. 1a), the digital micromirror device (DMD) acts as a "dynamic mask" to control the shape and size of the illuminated laser beam (Advanced Optowave Corporation, wavelength 355 nm, pulse duration 30 ns, and repetition rate 1 kHz) and thus the shape and size of the corresponding grating pixel, obtained from the interference pattern of one laser pulse. After transmitting through a 4F imaging system, the spatially modulated laser beam was split into ±1st order beams by a diffraction optical element (DOE, 1D micrometer-scale grating) and the two beams are subsequently collected by the objective lens to be focused onto the photoresist surface to yield the interference pattern. It has been theoretically demonstrated that the resultant periodicity p at the focused spot follows the equation $p = P/2M$, where P is the periodicity of the DOE and M is the magnification ratio of the objective lens.[32] In order to obtain feedback in the visible red regime using the second Bragg feedback, a subwavelength grating with a periodicity of around 400 nm is desired, and thus we have utilized an objective with a magnification ratio of 50 and a silica DOE with a periodicity of 40 μm. The DOE was further etched to a depth of around 380 nm to eliminate the 0th transmission at 355 nm, otherwise, the 0th transmission would overlap with the two diffractive beams inducing a low-quality interference pattern with a doubled periodicity. The system was also optimized to work in the pulsed mode, where one pixelated grating was completed by the interference pattern formed by the single laser pulse, yielding both high fabrication efficiency and excellent pattern stability. In addition, the distribution of these pixelated subwavelength gratings is precisely controlled by the stage with a position error of 0.1 μm, exhibiting great convenience for planar functionalization and integration.

In order to obtain the free-standing polymer film with nanoimprinted subwavelength gratings, we employed a route

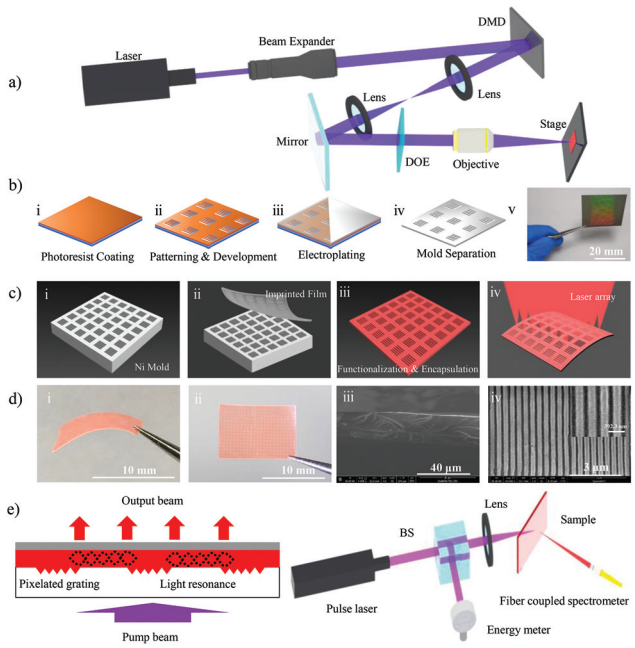

Fig. 1 Fabrication of the mechanically bendable and conformally attachable microcavity laser array based on the digital interference lithography technique. (a) Illustration of the optical setup of the digital interference lithography system. (b) Illustration of the fabrication process of the hard Ni mold including photoresist coating (i), patterning and development (ii), electroplating (iii), mold separation (iv) and the photograph of the Ni mold (v). (c) Illustration of the fabrication process of the free-standing microcavity laser array membrane including mold cleaning (i), imprinting using the UV-curable adhesive and the subsequent film peeling off (ii), functionalization and encapsulation *via* a subsequent coating of the active film and the encapsulation layer in sequence (iii), and the completed microcavity laser array polymer membrane (iv). (d) Characterization of the free-standing film with microcavities. End-view photograph of the membrane (i) and front-view photograph of the membrane (ii), where the iridescent regions correspond to the subwavelength grating pixels caused by light diffraction. End-view SEM image of the free-standing membrane (iii) and the SEM image showing the pixelated surface relief grating on the membrane, where the inset is the SEM image at a higher magnification (iv). (e) Schematic illustrations of the DBR microlaser array structure and the optical path for optical pumping of the membrane laser array.

to fabricate a hard Ni mold for the subsequent replication (Fig. 1b). Firstly, a positive photoresist (Suzhou Ruihong) film with a thickness of 200 nm was coated onto silica (Fig. 1b-i) and was patterned with pixelated interference patterns (the pixel width and length are both 60 μm and the horizontal and vertical spacings between the two adjacent pixels are both 120 μm) using the above system, yielding the desired pixelated subwavelength gratings with surface relief morphology after development (Fig. 1b-ii). Then the sample was immersed in the silver ammonia solution for the deposition of a thin silver seed layer covered on the relief gratings as a conducting layer and was then electroplated in a nickel plating bath (Fig. 1b-iii). The 1-inch size Ni plate with hundreds of grating pixels was then peeled off from the substrate with a complementary relief grating morphology (Fig. 1b-iv), which shows iridescent colors in the pixel regions due to the light diffraction after removing the residue photoresist (Fig. 1b-v). The thickness of the Ni plate could be controlled by the electroplating time and was around 300 μm to obtain both mechanical flexibility and reliability. A drop of the UV curable adhesive (H818, Quinson Adhesive) was then brought into contact with the obtained Ni mold (Fig. 1c-i) and was laminated by a non-stick plastic film for uniform coverage and was subsequently cured *via* a UV light source for 12 s (50 mW cm^{-2}, 365 nm). After photo-polymerization, the non-stick film was removed and the free-standing imprinted polymer film was peeled off from the Ni mold (Fig. 1c-ii), and was placed onto a substrate for the following gain medium coating. The blended conjugated polymers of the blue-emitting PFO (poly(9,9-dioctylfluorene), Sigma Aldrich, MW 20 000) and the red-emitting MEH-PPV (poly(2-methoxy-5-(2′-ethyl-hexyloxy)-*p*-phenylenevinylene), Sigma Aldrich, MW 200 000) at a weight ratio of 10 : 3 was dissolved in toluene at a total concentration of 1.2 wt% and was overcoated onto the imprinted polymer film to form a uniform conjugated polymer film of around 120 nm as the gain medium (Fig. 1c-iii). Subsequently, a second small drop of the UV adhesive was spread homogeneously onto the active film as laminated by a second non-stick plastic film and was exposed to the same UV light source for 12 seconds for photo-polymerization to form the protecting layer to encapsulate the microcavity laser array from oxygen and moisture, which leads to a free-standing polymer membrane with hundreds of polymer microlasers after removing the non-stick plastic film (Fig. 1c-iv).

The obtained free-standing polymer membrane with the microlaser array has advantages of both high mechanical flexibility and excellent performance reliability, as the film is free from the supporting substrate and encapsulated in the UV curable adhesives. The membrane was naturally bent at the tweezers' tip due to self-weight (Fig. 1d-i), indicating excellent softness and ultra-thin thickness; in addition, the microcavity laser array membrane could be non-destructively handled and transferred using the tweezers without resorting to additional handling substrates, exhibiting high convenience for characterization and application. The cross-sectional scanning electron microscopy (SEM) image of the polymer membrane (Fig. 1d-iii) reveals that the membrane has a total thickness of around 30 μm, which is less than half the thickness of a typical newspaper page, which is beneficial for excellent mechanical bendability and conformal attachability. In addition, the polymer membrane cross-section has two distinct textures, of which the thicker layer (around 20 μm) corresponds to the nanoimprinted polymer film to ensure a robust peeling off from the Ni mold while the thinner one corresponds to the laminated protective layer. It is also worth noting that the active conjugated polymer film is too thin to be distinguished from the presented SEM image. The front-view photograph of the polymer membrane (Fig. 1d-ii) under a slanted white illumination clearly illustrates the periodic distribution of replicated grating pixels. The morphology of the replicated subwavelength grating pixel on the photo-polymerizable

polymer film was also investigated (Fig. 1d-iv), which demonstrates a high quality grating composed of periodic straight line structures with a periodicity of 392.3 nm and an aspect ratio of 0.3, aiming to provide efficient feedback at the wavelength of around 610 nm with an approximated effective refractive index of around 1.55. The modulation depth of the imprinted pixelated grating was around 50 nm according to the atomic force microscopy measurement, which was found sufficient to provide effective optical feedback. Each pair of subwavelength gratings constitutes a DBR microcavity laser when the pump beam is focused onto the middle bare region, where each pixel is shared by two microcavities, acting as the Bragg mirror for the right and left microlaser simultaneously (Fig. 1e).

For photoluminescence measurement to reveal the resonating characteristics of the cavity, the single microcavity laser was pumped by focusing the coherent wave laser beam (1 mw, CrystaLaser) onto the region between the two Bragg gratings. Photoluminescence emission was collected using a 1 mm diameter fiber placed at a distance of 40 mm from the sample and investigated using the spectrometer (Avaspec, resolution 0.19 nm). The fiber was mounted on a circular track to collect emission from a range of polar angles normal to the sample plane. For lasing characterization, the sample was vertically mounted on a two-dimensional stage and pumped by the focused spots of the pulsed laser (Spectra Physics, wavelength 349 nm, pulse duration 8 ns, and repetition rate 10 Hz) using a quartz lens (Diameter 25.4 mm, focal length 20 cm). Normal emission to the sample surface in reference to the DBR microcavity laser in operation was collected (Fig. 1e) and analyzed by the same fiber coupled spectrometer. The strain along the grating vector was applied by mounting the polymer membrane using two clips and the pumping spot was maintained between the two grating pixels, where the normal emission was investigated using the spectrometer.

The microcavity laser array polymer membrane was completed when the pixelated subwavelength gratings were overcoated with the active organic semiconductor film of matched spectrum response, as the reflection lights resonating between every two grating pixels facing each other would be amplified when hitting the active molecules at the excited state through the stimulated emission process. In this work, the subwavelength grating pixels (60 μm) are distributed across the sample with the spacing between the adjacent pixels in both the horizontal and vertical directions being 120 μm, giving rise to a number of DBR microcavity lasers. These pixelated subwavelength relief gratings, which consists of periodic lines perpendicular to the surface, not only acted as the second-order Bragg mirrors for lights traveling in the surface plane, but also coupled the emitted light in the sample plane to the vertical direction of the sample *via* the first order grating effect.[33] The angle-dependent photoluminescence map could reveal the resonating properties of the microcavity (Fig. 2a), and it clearly showed that two emission bands anticross at an angle normal to the waveguide, giving rise to a wavelength dip at the anticrossing, indicating the resonating wavelength of the microcavity of around 620 nm.[33] To gain more insight into the feedback mechanism of the DBR microcavity, we have calculated the electric field intensity distribution of the eigen modes in the region between the two grating pixels using the finite element method (*i.e.*, COMSOL Multiphysics software) (Fig. 2b). Strong resonation was observed at the operating wavelength of 620 nm with a complete confinement of light inside the active film acting as the waveguide layer, while light was distributed homogeneously with a low intensity in the active layer at a detuning wavelength of 600 nm, implying the superior wavelength selection mechanism of the microcavity. As for pulsed pumping to investigate the lasing performance, the spectrum of emission from each DBR microcavity laser on the membrane undergoes a significant change (Fig. 2c) when the pump fluence increases step by step, *i.e.*, only a broad spectrum with two characteristic shoulder peaks referring to spontaneous emission when the pump fluence is below 15 μJ cm^{-2}, a low intensity narrow lasing peak at around 620 nm being superimposed onto broad spontaneous emission when the pump fluence is between 15 μJ cm^{-2} and 18 μJ cm^{-2}, and the domination of the lasing peak over spontaneous emission when the pump fluence is above 18 μJ cm^{-2}, presenting a clear transition from spontaneous emission to stimulated emission as the cavity loss is surpassed by the increased gain at a higher pump fluence. For a quantitative illustration of the emission transition, we have also provided the evolution of the peak intensity and the full width at half maxima (FWHM) of the main emission peak along with the pump fluence (Fig. 2d). As

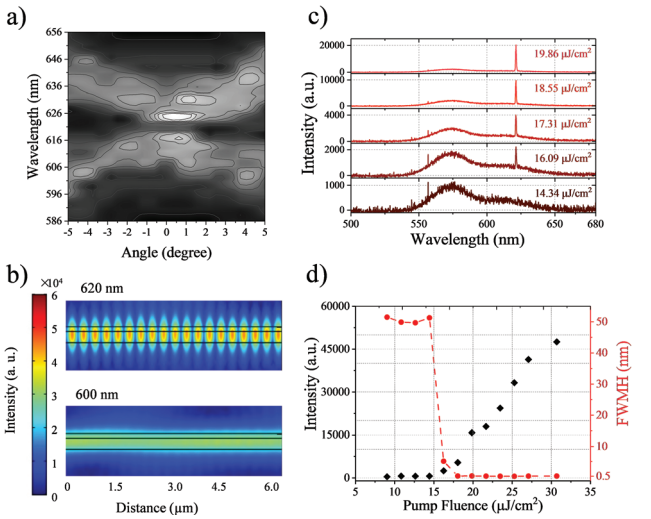

Fig. 2 Resonating characterization of the single DBR microcavity. (a) Interpolated gray scale image of the angle-dependent photoluminescence. (b) The electric field intensity distribution of the eigen modes in the region between the two grating pixels at the resonating wavelength (620 nm) and at the detuning wavelength (600 nm). (c) The evolution of the emission spectrum to the sample normal with the pump fluence for one DBR microcavity laser on the membrane, indicating the transition from the spontaneous emission to lasing. (d) Output intensity and FWHM of normal emission as a function of the pump fluence for one DBR microcavity laser on the membrane.

the pump fluence goes up, the peak emission intensity first increases linearly at a very slow rate, due to the omnidirectionality characteristic of spontaneous emission, and at some point, it undergoes an abrupt rise and follows the linear curve with a much higher slope efficiency, attributing to the directionality of the stimulated emission, indicating the onset of laser emission. Correspondingly, the FWHM stays around 50 nm and undergoes a sudden sharping to below 1 nm when the emission intensity abruptly changes, also presenting a working threshold of around 15.5 μJ cm^{-2}.

Apart from the low threshold, the DBR microcavity laser on the polymer membrane also appears high performance reliability, which shows stable narrow laser emission after being stored for two months (Fig. 3a), demonstrating the robustability of the soft microcavity laser array polymer membrane for long-time working and arbitrary transferring purposes. We have further measured the laser emission from different DBR microcavity lasers on the polymer membrane to check the uniformity of the fabricated laser array, where the lasing wavelength varies between 618.5 nm and 621.5 nm depending on the detected location (Fig. 3b) while the working threshold stays around 16 μJ cm^{-2}. The distribution of the lasing wavelength is not random but has a clear dependence on the position on the membrane, implying that the variation in the lasing wavelength across the array is a result of the thickness inhomogeneity in the spin-coated active film but not the periodicity inaccuracy in these pixelated subwavelength gratings, demonstrating the high reliability and accuracy of the digital interference lithography system in providing subwavelength grating pixels. It is worth noting that the number of output laser beams and the intensity of each laser beam could be controlled by the size and intensity distribution of the pumping region, enabling a multiple-microlaser chip. From the photographs of the output lasing patterns captured using a CCD camera at a distance of 4 mm and 12 mm (Fig. 3c), it can be deduced that the divergence angle of the DBR microcavity laser is around 12 mrad and 48 mrad in the horizontal and vertical directions, respectively. In the planar DBR microcavity laser, light at the oscillating wavelength resonates in the sample plane *via* the second order Bragg effect while it is coupled out to the normal direction by the first order grating effect, furnishing a vertically emitting microcavity laser array on the polymer membrane for convenient light coupling and utilization. The strain-dependent emitting wavelength of the microlaser on the ultra-thin polymer membrane further demonstrated the potential of the soft membrane as a natural tunable laser source (Fig. 3d). The lasing wavelength could be tuned reversibly from 621 nm to 630 nm by applying the axial strain, which was attributed to the elongation of the grating period. In addition, the wavelength tuning range could be expanded by optimizing the elastomeric properties of the cured adhesive.

Such a thin microcavity laser array polymer membrane with high toughness is potentially extremely mechanically flexible and performance stable, which could be exploited to use in wearable electronics or outdoor environmental monitoring. In order to investigate the effects of conformal attaching on irregular surfaces and repeatable bending circles on device performance, the output lasing spectra and the corresponding laser thresholds were recorded in different attaching and bending circumstances (Fig. 4). The polymer membrane was

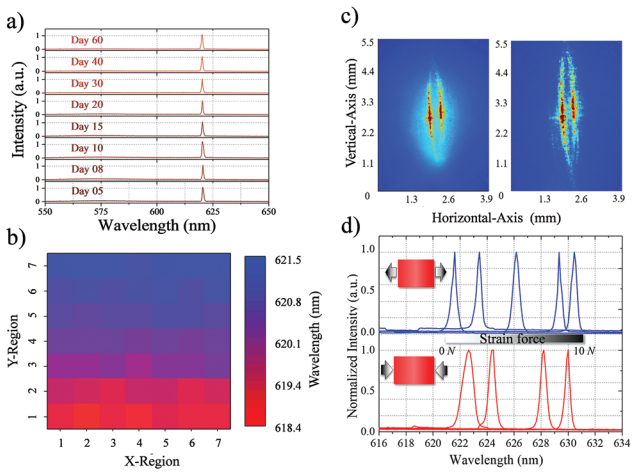

Fig. 3 Lasing performance of the polymer membrane microlaser array. (a) The lasing spectra from one DBR microcavity laser on the membrane pumped under a fluence of 18 μJ cm^{-2} at different storage days. (b) The distribution of the lasing wavelength emitted from the DBR microcavity laser array on the membrane. (c) CCD image of the lasing spot emitted from one DBR microcavity laser on the membrane at a distance of 4 mm (the upper panel) and 12 mm (the lower panel). (d) Dependence of the output lasing wavelength from one microlaser on the applied axial strain.

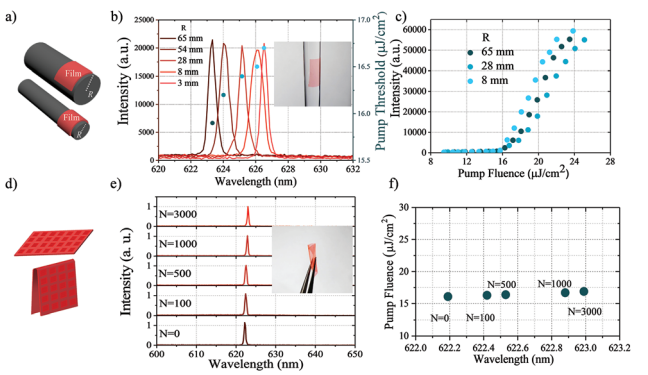

Fig. 4 Mechanical flexibility and bendability performance of the microcavity laser array polymer membrane. (a) Schematic illustration for the attaching operation of the polymer membrane on rounded objects with different radii. (b) The lasing spectrum and the working threshold of the single DBR microcavity laser when the polymer membrane was attached on a rounded object as a function of radius. The inset is a photograph of the polymer membrane attached on a curved object. (c) Emission intensity as a function of pump fluence for single DBR microcavity laser when the polymer membrane was attached on different rounded objects with radii of 65 mm, 28 mm and 8 mm. (d) Schematic illustration of the mechanical bending operation of the microcavity laser array polymer membrane. (e) Emission spectra from the single DBR microcavity laser when the polymer membrane was bent for different circles. The inset is a photograph of the polymer membrane being bent. (f) The lasing wavelength and the working threshold of the single DBR microcavity as a function of the bending number of the polymer membrane.

transferred and attached onto cylindrical objects with different cross-sectional radii and was mounted on a stage for lasing performance characterization (Fig. 4a). The membrane transfer onto the irregular surface was operated directly with a tweezer and was initially moved onto the surface with the aid of deionized water, leaving a conformally attached membrane after the evaporation of the solvent due to the ultra-thin thickness and excellent softness of the film. The membrane exhibited well-defined single-mode lasing characteristic with the FWHM of the lasing peak being well below 1 nm irrespective of the radius of the attaching surface (Fig. 4b), due to the preserved optical confinement of the lasing mode in the active film at such a small membrane thickness, *i.e.*, the active film preserved original physical and chemical properties when the thin membrane was bent or curved along with different surface morphologies. The lasing wavelength increased slightly from 623.33 nm to 626.51 nm as the attaching radius of the cylindrical object decreased from 65 mm to 3 mm with recovery capability, probably due to the slightly elongated grating pitch at the high bending curvature. In addition, the microcavity laser array exhibited excellent lasing performance and the threshold slightly fluctuated in the range between 16 μJ cm^{-2} and 17 μJ cm^{-2} (Fig. 4b and c), implying the reliability and robustability of the ultra-thin polymer membrane as a mechanically flexible microcavity laser array. In order to further explore the potential of the microcavity laser polymer membrane to implement in harsher application scenarios requiring extreme flexibility, a severe bending test was carried out, in which the polymer membrane was bent to a radius of 0.5 mm and then spread flat repeatedly (Fig. 4d). The laser emission maintained the single-mode performance when the bending number is up to 3000, with a very slight red-shift in the lasing wavelength from 622.2 nm to 623.0 nm (Fig. 4e), as a result of the hysteresis effect in the grating morphology recovery while the membrane was being repeatedly bent and released. The device working threshold stayed almost unchanged during the whole bending operation (Fig. 4f), as the nanometer-scale active film was uniformly encapsulated and protected by micrometer-scale adhesive films, again demonstrating the reliability of the ultra-thin polymer microcavity laser membrane for bending and attaching purposes.

The ultra-thin thickness of the microcavity laser array polymer membrane, in combination with its potential compatibility with organic materials, drives us to explore its potential in wearable or disposable electronics, *i.e.*, as the wearable security tag for biometric authentication or the disposable laser for outdoor environmental monitoring and was investigated subsequently by attaching the membrane on the contact lens and the human nail (Fig. 5a and b). The membrane was conformally placed onto the contact lens and the human nail, in addition, after the evaporation of the transferring solution such as deionized water, the membrane was found to be firmly adhered on the irregular surface due to the surface tension and compatibility of the polymer membrane with the biological tissues (Fig. 5a-i and b-i). When the ultra-violet pulsed laser was focused onto the polymer membrane, either covering

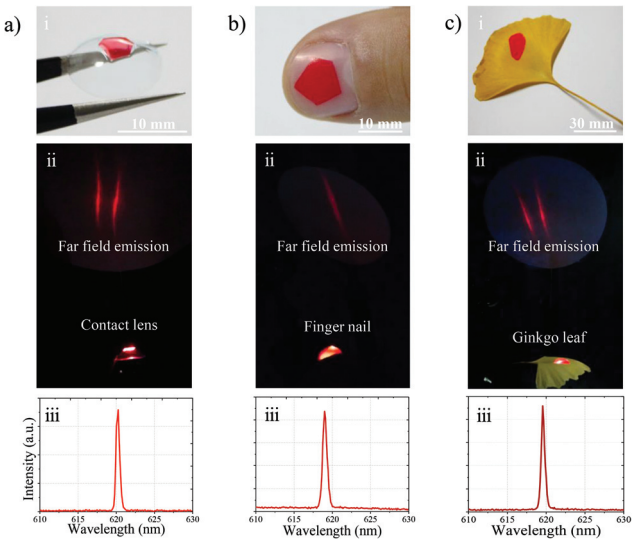

Fig. 5 Conformal attachability of the microcavity laser array membrane on objects with different curvatures. The polymer membrane attached on (a) the contact lens, (b) the nail and (c) the gingko leaf. The upper, middle and lower panels illustrate the photographs of the microcavity laser membrane on the corresponding curved object, the photographs of laser emission from the microcavity laser membrane on corresponding curved object and the lasing spectrum from the microcavity laser membrane on the corresponding curved object, respectively.

one region between two grating pixels to stimulate one microcavity laser or some regions between different pixels to stimulate multiple ones, the polymer membrane on the biological tissue would emit directional lasing patterns (Fig. 5a-ii and b-ii), just as the typical second-order DBR laser, while still preserving the good single mode lasing characteristic at around 620 nm (Fig. 5a-iii and b-iii). As the active organic semiconductor film was sandwiched between the photo-polymerized imprinted film and the encapsulation film, the intensity distribution of the lasing mode and thus its optical confinement inside the active film would stay the same, irrespective of the substrate material being transferred on, thereby ensuring high performance and stable lasing operation in different application scenarios. In addition, the DBR microcavity laser array requires a very low pump power density of around 2 kW cm^{-2} for operation and such a low pump density, especially after the major energy being absorbed by the active material, would be far below the damage threshold of some biological tissues (Fig. 5b-ii indicates a laser emitting finger nail and no tissue damage was observed during the test), indicating the practical feasibility of the microcavity membrane for wearable laser devices. To further investigate the compatibility of the microcavity laser array polymer membrane with plants and explore the possible use in outdoor environmental monitoring, the membrane was transferred onto a ginkgo leaf and it was also found to be conformally attached, without influencing the original plant morphology (Fig. 5c-i). Under suitable optical pumping, the leaf emitted a directional lasing pattern with excellent single mode characteristic (Fig. 5c-ii and iii), where the lasing threshold increased slightly by 5% after a continu-

ous emission duration of ten minutes, showing stable lasing operation. In addition, the leaf still preserved the biological characteristics after the long-time operation as a result of the low pump irradiance, indicating the potential of the polymer membrane as the disposable laser for outdoor environmental monitoring.

Conclusions

In this work, we have presented a mechanically bendable and conformally attachable microcavity laser array membrane exhibiting excellent lasing performance based on the digital interference lithography technique. The developed lithography system is capable of patterning subwavelength grating pixels in the pulse mode with an efficiency of 1k pixels per second; in addition, the pixel parameters such as the size, the shape, the location and the grating periodicity would be controlled in a precise and simple manner, acting as a powerful platform for optical functionalization and integration. As a demonstration, we have distributed hundreds of subwavelength grating pixels with the size and periodicity being 60 μm and 392.3 nm on the plane, respectively, in which each pair of subwavelength gratings constitutes a DBR microcavity laser, resulting in a vertically emitting microcavity laser array with a low working threshold of around 15 μJ cm^{-2}. The free-standing microlaser array polymer membrane with ultra-thin thickness (30 μm, less than half thickness of a typical newspaper page), in combination with its potential compatibility with organic materials,[34] opens the possibility to be reversibly stretched, repeatedly bent or to be conformally attached onto different irregular surfaces or biological tissues, such as the contact lens, the finger nail and the ginkgo leaf, without the degradation in single-mode or low-threshold laser characteristics, paving a way to implement the PICs in wearable or disposable electronics.

Conflicts of interest

There are no conflicts to declare.

Acknowledgements

We are grateful for the financial support from the National Natural Science Foundation of China (NSFC) (61575135 and 61505131) and the Natural Science Foundation of Jiangsu Province (BK20150309).

Notes and references

1 R. Bruck, B. Mills, B. Troia, D. J. Thomson, F. Y. Gardes, Y. Hu, G. Z. Mashanovich, V. M. N. Passaro, G. T. Reed and O. L. Muskens, *Nat. Photonics*, 2015, **9**, 54–60.
2 Y.-Q. Bie, G. Grosso, M. Heuck, M. M. Furchi, Y. Cao, J. Zheng, D. Bunandar, E. Navarro-Moratalla, L. Zhou, D. K. Efetov, T. Taniguchi, K. Watanabe, J. Kong, D. Englund and P. Jarillo-Herrero, *Nat. Nanotechnol.*, 2017, **12**, 1124–1129.
3 M. Davanco, J. Liu, L. Sapienza, C.-Z. Zhang, J. V. De Miranda Cardoso, V. Verma, R. Mirin, S. W. Nam, L. Liu and K. Srinivasan, *Nat. Commun.*, 2017, **8**, 889.
4 C. Monat, P. Domachuk and B. J. Eggleton, *Nat. Photonics*, 2007, **1**, 106–114.
5 J. Hu, L. Li, H. Lin, P. Zhang, W. Zhou and Z. Ma, *Opt. Mater. Express*, 2013, **3**, 1313–1331.
6 L. Eldada and L. W. Shacklette, *IEEE J. Sel. Top. Quantum Electron.*, 2000, **6**, 54–68.
7 S. Aikio, J. Hiltunen, J. Hiitola-Keinänen, M. Hiltunen, V. Kontturi, S. Siitonen, J. Puustinen and P. Karioja, *Opt. Express*, 2016, **24**, 2527–2541.
8 V. Bonal, R. Muñoz-Mármol, F. G. Gámez, M. Morales-Vidal, J. M. Villalvilla, P. G. Boj, J. A. Quintana, Y. Gu, J. Wu, J. Casado and M. A. Díaz-García, *Nat. Commun.*, 2019, **10**, 3327.
9 M. C. Gather and S. H. Yun, *Nat. Commun.*, 2014, **5**, 5722.
10 H. Kubota, S. Oomi, H. Yoshioka, H. Watanabe and Y. Oki, *Opt. Express*, 2012, **20**, 14938–14944.
11 J. Herrnsdorf, B. Guilhabert, Y. Chen, A. L. Kanibolotsky, A. R. Mackintosh, R. A. Pethrick, P. J. Skabara, E. Gu, N. Laurand and M. D. Dawson, *Opt. Express*, 2010, **18**, 25535–25545.
12 Y. Chen, J. Herrnsdorf, B. Guilhabert, A. L. Kanibolotsky, A. R. Mackintosh, Y. Wang, R. A. Pethrick, E. Gu, G. A. Turnbull, P. J. Skabara, I. D. W. Samuel, N. Laurand and M. D. Dawson, *Org. Electron.*, 2011, **12**, 62–69.
13 C. Foucher, B. Guilhabert, J. Herrnsdorf, N. Laurand and M. D. Dawson, *Opt. Express*, 2014, **22**, 24160–24168.
14 H.-H. Fang, R. Ding, S.-Y. Lu, X.-L. Zhang, J. Feng, Q.-D. Chen and H.-B. Sun, *J. Mater. Chem.*, 2012, **22**, 24139–24144.
15 S. Schauer, X. Liu, M. Worgull, U. Lemmer and H. Hölscher, *Opt. Mater. Express*, 2015, **5**, 576–584.
16 A. Berdin, H. Rekola, O. Sakhno, M. Wegener and A. Priimagi, *Opt. Express*, 2019, **27**, 25634–25646.
17 C. Foucher, B. Guilhabert, A. L. Kanibolotsky, P. J. Skabara, N. Laurand and M. D. Dawson, *Opt. Express*, 2016, **24**, 2273–2280.
18 M. Karl, J. M. E. Glackin, M. Schubert, N. M. Kronenberg, G. A. Turnbull, I. D. W. Samuel and M. C. Gather, *Nat. Commun.*, 2018, **9**, 1525.
19 T. Zhai, Y. Wang, L. Chen, X. Wu, S. Li and X. Zhang, *Nanoscale*, 2015, **7**, 19935–19939.
20 T. Zhai, Z. Xu, X. Wu, Y. Wang, F. Liu and X. Zhang, *Opt. Express*, 2016, **24**, 437–442.
21 J. B. Wright, S. Liu, G. T. Wang, Q. Li, A. Benz, D. D. Koleske, P. Lu, H. Xu, L. Lester, T. S. Luk, I. Brener and G. Subramania, *Sci. Rep.*, 2013, **3**, 2982.
22 A. Yang, T. B. Hoang, M. Dridi, C. Deeb, M. H. Mikkelsen, G. C. Schatz and T. W. Odom, *Nat. Commun.*, 2015, **6**, 6939.
23 X. Liu, S. Prinz, H. Besser, W. Pfleging, M. Wissmann, C. Vannahme, M. Guttmann, T. Mappes, S. Koeber,

C. Koosbe and U. Lemmer, *Faraday Discuss.*, 2014, **174**, 153–164.
24 A. Yang, T. B. Hoang, M. Dridi, C. Deed, M. H. Mikkelsen, G. C. Schatz and T. W. Odom, *Nat. Commun.*, 2015, **6**, 6939.
25 B. Guilhabert, N. Laurand, J. Herrnsdorf, Y. Chen, A. L. Kanibolotsky, C. Orofino, P. J. Skabara and M. D. Dawson, *IEEE Photonics J.*, 2012, **4**, 684–690.
26 Z. Dong, J. Ho, Y. F. Yu, Y. H. Fu, R. Paniagua-Dominguez, S. Wang, A. I. Kuznetsov and J. K. W. Yang, *Nano Lett.*, 2017, **17**, 7620–7628.
27 Y. Nagasaki, M. Suzuki and J. Takahara, *Nano Lett.*, 2017, **17**, 7500–7506.
28 K. Yamashita, H. Yanagi and K. Oe, *Opt. Lett.*, 2011, **36**, 1875–1877.
29 Q. Liao, X. Jin, H. Zhang, Z. Xu, J. Yao and H. Fu, *Angew. Chem., Int. Ed.*, 2015, **54**, 7037–7041.
30 J. Feng, X. Jiang, X. Yan, Y. Wu, B. Su, H. Fu, J. Yao and L. Jiang, *Adv. Mater.*, 2016, **29**, 1603652.
31 C. Zhang, C.-L. Zou, Y. Zhao, C.-H. Dong, C. Wei, H. Wang, Y. Liu, G.-C. Guo, J. Yao and Y. S. Zhao, *Sci. Adv.*, 2015, **1**, e1500257.
32 Y. Ye, F. Xu, G. Wei, Y. Xu, D. Pu, L. Chen and Z. Huang, *Opt. Lett.*, 2017, **42**, 1978–1981.
33 G. A. Turnbull, P. Andrew, M. J. Jory, W. L. Barnes and I. D. W. Samuel, *Phys. Rev. B: Condens. Matter Mater. Phys.*, 2001, **64**, 125122.
34 M. Berggren, D. Nilsson and N. D. Robinson, *Nat. Mater.*, 2007, **6**, 3–5.